

Multipolar response of nonspherical silicon nanoparticles in the visible and near-infrared spectral ranges

Pavel D. Terekhov,^{1,2,*} Kseniia V. Baryshnikova,² Yuriy A. Artemyev,^{1,2} Alina Karabchevsky,^{1,†} Alexander S. Shalin,² and Andrey B. Evlyukhin^{2,3}

¹*Electrooptical Engineering Unit and Ilse Katz Institute for Nanoscale Science & Technology, Ben-Gurion University, Beer-Sheva 84105, Israel*

²*ITMO University, 49 Kronversky Ave., 197101 St. Petersburg, Russia*

³*Laser Zentrum Hannover e.V., Hollerithallee, D-30419 Hannover, Germany*

(Received 26 May 2017; revised manuscript received 13 July 2017; published 31 July 2017)

Spectral multipole resonances of parallelepiped-, pyramid-, and cone-like shaped silicon nanoparticles excited by linearly polarized light waves are theoretically investigated. The numerical finite element method is applied for the calculations of the scattering cross sections as a function of the nanoparticles geometrical parameters. The roles of multipole moments (up to the third order) in the scattering process are analyzed using the semianalytical multipole decomposition approach. The possibility of scattering pattern configuration due to the tuning of the multipole contributions to the total scattered waves is discussed and demonstrated. It is shown that cubic nanoparticles can provide a strong isotropic side scattering with minimization of the scattering in forward and backward directions. In the case of the pyramidal and conical nanoparticles the total suppression of the side scattering can be obtained. It was found that due to the shape factor of the pyramidal and conical nanoparticles their electric toroidal dipole resonance can be excited in the spectral region of the first electric and magnetic dipole resonances. The influence of the incident light directions on the optical response of the pyramidal and conical nanoparticles is discussed. The obtained results provide important information that can be used for the development of nanoantennas with improved functionality due to the directional scattering effects.

DOI: [10.1103/PhysRevB.96.035443](https://doi.org/10.1103/PhysRevB.96.035443)

I. INTRODUCTION

Optical properties of high-refractive-index dielectric nanoparticles have attracted great scientific interest during the past several years [1–6]. These subwavelength scatterers can support the excitation of electric and magnetic multipolar resonances [1–7] which enhance the light-matter interaction in a controllable manner by changing the nanoparticles size, geometry, and material [7,8]. Compared to the plasmonic nanoparticles, which reveal novel optical phenomena due to change in optical density of states [9,10], all-dielectric nanoantennas do not exhibit Joule losses. Desirable overlapping of certain multipole resonances of the dielectric nanoparticles can be used for different applications, including nanoantennas [11–14], sensors [15,16], solar cell technology [17], and multifunctional metasurfaces [18]. For example, directional light scattering due to the resonant Kerker effect (the overlapping of the electric and magnetic dipole resonances) [19] in the dielectric nanodisks has been used for the experimental realization of Huygens metasurfaces [18,20,21]. Recently, resonant directional light scattering induced by the third order multipoles contribution in dielectric nanocylinders has been investigated [22]. A multipolar light-matter interaction has been also demonstrated by modifying configuration of the illuminating radiation applied on a nanoscatterer with selective excitation of individual multipole modes [23].

Silicon is one of the most suitable materials for the resonant dielectric nanophotonics [1–3,8,21]. In different crystallographic states silicon provides a large refractive index and

negligible absorption losses in the near-infrared spectral range. In the visible spectral range, however, the absorption increases [24]. For this reason, the propagation length of monochromatic red light approaches several microns in bulk crystalline silicon. However, if the size of silicon nanoparticles is significantly smaller compared to the light propagation length, the absorption by such a particle can be neglected. In this case, the light extinction is mainly determined by the light scattering effect. Therefore, the silicon nanoparticles can be considered as dielectric nanoparticles in the visible spectral range.

In this work we investigate spectral multipole resonances of parallelepiped-, pyramid-, and cone-like shaped silicon nanoparticles excited by the linear polarized light waves (Fig. 1). In contrast to previous work, where resonant dipole responses are basically considered in silicon nanostructures, here we pay attention to the higher order multipoles (up to the third order) and their role in the scattering pattern configuration. The information on the multipole response of the parallelepiped-, pyramid-, and cone-like nanoparticles is important, e.g., for the development of multifunctional nanoantennas. Note that small deviations from the ideal shape can appear during fabrication procedures. However, optical properties of dielectric particles are expected to be weak sensitive to these small shape deviations, because electromagnetic field concentrates inside the particle volume (for example [25]). Our theoretical study is based on the numerical finite element method, implemented in COMSOL Multiphysics, and on the semianalytical multipole decomposition method [26,27].

II. THEORETICAL BACKGROUND

Our theoretical analysis is based on the multipole decomposition method developed for the light scattering by

*terekhovpd@gmail.com

†alinak@bgu.ac.il

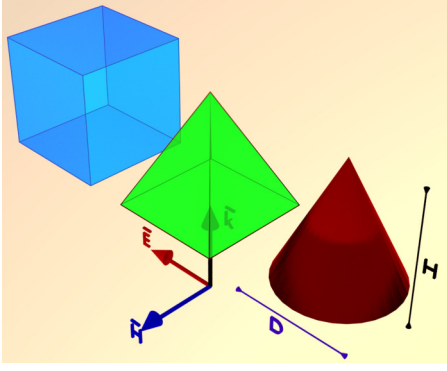


FIG. 1. Artistic representation of the silicon nanoscatterers geometry explored in this study: parallelepiped, pyramid, and cone with varying height H and diameter of $D = 250$ nm. \mathbf{k} is the wave vector of the incident light, \mathbf{E} is the electric field, and \mathbf{H} (\vec{H}) is the magnetic field.

arbitrary-shaped nanoparticles [26] where the multipole contributions (up to the third order) to the scattering cross section have been considered. Briefly, the multipole moments of a scatterer are determined by the polarization $\mathbf{P} = \varepsilon_0(\varepsilon_p - \varepsilon_d)\mathbf{E}$, induced by the incident light wave, where ε_0 , ε_p , ε_d are the vacuum dielectric constant, relative dielectric permittivity of the particle, and relative dielectric permittivity of the surrounding medium, respectively; \mathbf{E} is the total electric field inside the scatterer. We consider that the time-dependent incident plane monochromatic wave is defined by $\exp(-i\omega t)$, where ω is the angular frequency, and is scattered by a single nanoparticle with its multipoles located at the origin of the Cartesian coordinate system coinciding with the nanoparticle's center of mass. Under these conditions the ordinary electric dipole (ED) moment of the scatterer is calculated as

$$\mathbf{p} = \int_V \varepsilon_0(\varepsilon_p - \varepsilon_d)\mathbf{E}(\mathbf{r}')d\mathbf{r}', \quad (1)$$

where V is the scatterer volume and \mathbf{r}' is the radius vector of a volume element inside the scatterer. The magnetic dipole (MD) moment of a scatterer is

$$\mathbf{m} = -\frac{i\omega}{2} \int_V \varepsilon_0(\varepsilon_p - \varepsilon_d)[\mathbf{r}' \times \mathbf{E}(\mathbf{r}')]d\mathbf{r}', \quad (2)$$

irreducible electric quadrupole (EQ) tensor (\hat{U} is the 3×3 unit tensor) of a scatterer is

$$\hat{Q} = 3 \int_V \varepsilon_0(\varepsilon_p - \varepsilon_d) \left[\mathbf{r}'\mathbf{E}(\mathbf{r}') + \mathbf{E}(\mathbf{r}')\mathbf{r}' - \frac{2}{3}(\mathbf{r}' \cdot \mathbf{E}(\mathbf{r}'))\hat{U} \right] d\mathbf{r}', \quad (3)$$

irreducible magnetic quadrupole (MQ) tensor of a scatterer is

$$\hat{M} = \frac{\omega}{3i} \int_V \varepsilon_0(\varepsilon_p - \varepsilon_d) \{ [\mathbf{r}' \times \mathbf{E}(\mathbf{r}')]\mathbf{r}' + \mathbf{r}'[\mathbf{r}' \times \mathbf{E}(\mathbf{r}')] \} d\mathbf{r}', \quad (4)$$

irreducible electric octupole (OCT) tensor \hat{O} of a scatterer is a tensor with components

$$O_{\beta\gamma\tau} = O'_{\beta\gamma\tau} - (\delta_{\beta\gamma}V_\tau + \delta_{\beta\tau}V_\gamma + \delta_{\gamma\tau}V_\beta), \quad (5)$$

where each index $\beta = x, y, z$, $\gamma = x, y, z$, and $\tau = x, y, z$, $\delta_{\alpha\beta}$ is the Kronecker delta, the tensor \hat{O}' is

$$\hat{O}' = \varepsilon_0 \int_V (\varepsilon_p - \varepsilon_d) \{ \mathbf{E}(\mathbf{r}')\mathbf{r}'\mathbf{r}' + \mathbf{r}'\mathbf{E}(\mathbf{r}')\mathbf{r}' + \mathbf{r}'\mathbf{r}'\mathbf{E}(\mathbf{r}') \} d\mathbf{r}', \quad (6)$$

and the vector \mathbf{V} is determined by the expression

$$\mathbf{V} = \frac{\varepsilon_0}{5} \int_V (\varepsilon_p - \varepsilon_d) \{ 2(\mathbf{r}' \cdot \mathbf{E}(\mathbf{r}'))\mathbf{r}' + (\mathbf{r}')^2\mathbf{E}(\mathbf{r}') \} d\mathbf{r}'. \quad (7)$$

The toroidal dipole (TD) moment, having the same radiation pattern as an electric dipole moment [28–30], is determined as

$$\mathbf{T} = \frac{i\omega}{10} \int_V \varepsilon_0(\varepsilon_p - \varepsilon_d) \{ 2\mathbf{r}'^2\mathbf{E}(\mathbf{r}') - (\mathbf{r}' \cdot \mathbf{E}(\mathbf{r}'))\mathbf{r}' \} d\mathbf{r}'. \quad (8)$$

Scattering patterns are determined by the differential scattering cross section σ_d corresponding to the normalized power dP_{sca} scattered into the solid angle $d\Omega = \sin\theta d\theta d\varphi$, where θ and φ are the polar and azimuthal angles of the spherical coordinate system, respectively [31]. The scattered power is normalized by the incident wave intensity. From this definition of σ_d one obtains

$$\sigma_d(\varphi, \theta) = \frac{dP_{\text{sca}}}{d\Omega} = \frac{|\mathbf{E}_0^{\text{sca}}(\mathbf{n})|^2}{|\mathbf{E}_{\text{inc}}|^2}, \quad (9)$$

where \mathbf{E}_{inc} is the electric field amplitude of the incident plane wave and

$$\begin{aligned} \mathbf{E}_0^{\text{sca}}(\mathbf{n}) \simeq & \frac{k_0^2}{4\pi\varepsilon_0} \left([\mathbf{n} \times [\mathbf{D} \times \mathbf{n}]] + \frac{1}{v_d} [\mathbf{m} \times \mathbf{n}] \right. \\ & + \frac{ik_d}{6} [\mathbf{n} \times [\mathbf{n} \times \hat{Q}\mathbf{n}]] + \frac{ik_d}{2v_d} [\mathbf{n} \times (\hat{M}\mathbf{n})] \\ & \left. + \frac{k_d^2}{6} [\mathbf{n} \times [\mathbf{n} \times \hat{O}(\mathbf{n}\mathbf{n})]] \right) \end{aligned} \quad (10)$$

is the electric field amplitude of the scattered spherical wave along the unit vector $\mathbf{n} = (\cos\varphi \sin\theta, \sin\varphi \sin\theta, \cos\theta)$, where k_0 and k_d are the wave numbers in vacuum and in surrounding media with ε_d , respectively, and v_d is the light velocity in the same surrounding medium.

The term

$$\mathbf{D} = \mathbf{p} + i \frac{k_d}{v_d} \mathbf{T} \quad (11)$$

in (10) includes the interference of electric dipole (ED) and electric toroidal dipole (TD) moments and can be treated as total electric dipole moment (TED). In the general case high-order terms can provide additional contributions beyond toroidal dipole with the same radiation pattern [32]. However, in our approximation it is enough to take into account only additional toroidal dipole contribution. Note that tensors \hat{Q} , \hat{M} , and \hat{O} are symmetric and traceless as can be found in the textbooks [27,33].

The scattering cross section σ_{sca} is determined by the equation

$$\sigma_{\text{sca}} = \int_0^\pi \int_0^{2\pi} \sigma_d(\theta, \varphi) d\Omega. \quad (12)$$

After the integration in (12), using (10), one obtains [26]

$$\begin{aligned} \sigma_{\text{sca}} \simeq & \frac{k_0^4}{6\pi \varepsilon_0^2 |\mathbf{E}_{\text{inc}}|^2} |\mathbf{D}|^2 + \frac{k_0^4 \varepsilon_d \mu_0}{6\pi \varepsilon_0 |\mathbf{E}_{\text{inc}}|^2} |\mathbf{m}|^2 + \frac{k_0^6 \varepsilon_d}{720\pi \varepsilon_0^2 |\mathbf{E}_{\text{inc}}|^2} \\ & \times \sum |\hat{Q}_{\alpha\beta}|^2 + \frac{k_0^6 \varepsilon_d^2 \mu_0}{80\pi \varepsilon_0 |\mathbf{E}_{\text{inc}}|^2} \sum |\hat{M}_{\alpha\beta}|^2 \\ & + \frac{k_0^8 \varepsilon_d^2}{1890\pi \varepsilon_0^2 |\mathbf{E}_{\text{inc}}|^2} \sum |\hat{O}_{\alpha\beta\gamma}|^2, \end{aligned} \quad (13)$$

where μ_0 is the vacuum permeability.

First, in our investigation total electric fields in scatterers and the corresponding scattering patterns are calculated numerically using finite element method (FEM) in COMSOL Multiphysics. The multipole moments are calculated following their definitions [Eqs. (1)–(8)]. Finally, the multipole decomposition of total scattering cross section σ_{scat} is obtained using Eq. (13).

III. LIGHT SCATTERING BY SILICON NANOPARTICLES

In this paper we consider light scattering on three nonspherically shaped particles, namely, on a parallelepiped, pyramid, and cone. Note that nanoparticles of these shapes can be fabricated by different approaches such as, e.g., focused ion beam (FIB) milling [34]. In contrast to the previous investigations [23,25,35] here we pay attention to the second- and third-order multipoles (resonant and nonresonant) contributions to the scattering. The dielectric permittivity of silicon was taken from the textbook [24]. In this article we consider that all nanoparticles are placed in a homogeneous surrounding medium with $\varepsilon_d = 1$.

A. Parallelepipedal nanoparticles

We start from the multipolar decomposition of the light scattering cross-section spectrum obtained from the cubic particle with height of $H = 250$ nm shown in Fig. 2. There are several spectral signatures (indicated by the black arrows) for which far-field radiation patterns have been calculated and shown in Fig. 3. Figure 2 demonstrates that the higher-order multipole resonances are excited with decreasing the light wavelength. It is worth noting that all resonances in Fig. 2 correspond to particular multipole moments resonantly excited by light. No total overlapping of several multipole resonances is realized. From Fig. 2 one can see that the electric quadrupole (EQ) resonances are excited at the wavelengths $\lambda = 619$ nm and $\lambda = 704$ nm, whereas a narrow magnetic dipole (MD) resonance is just between them. The magnetic quadrupole (MQ) resonant contribution provides a pronounced peak at the wavelength of $\lambda = 765$ nm. Moreover, the usual and well-known peaks provided by TED and MD take place at $\lambda = 900$ nm and $\lambda = 1140$ nm correspondingly. Note that good agreement between total cross-section and multipole sum are saved for all the considered particle shapes.

The far-field radiation patterns which correspond to the EQ and MQ resonances are shown in Figs. 3(a)–3(c). It is clearly seen that there are four radiation lobes corresponding to the forward, backward, and side scattering. In the case of the EQ (MQ) resonances the side lobes are oriented along the electric (magnetic) field polarization in the incident plane

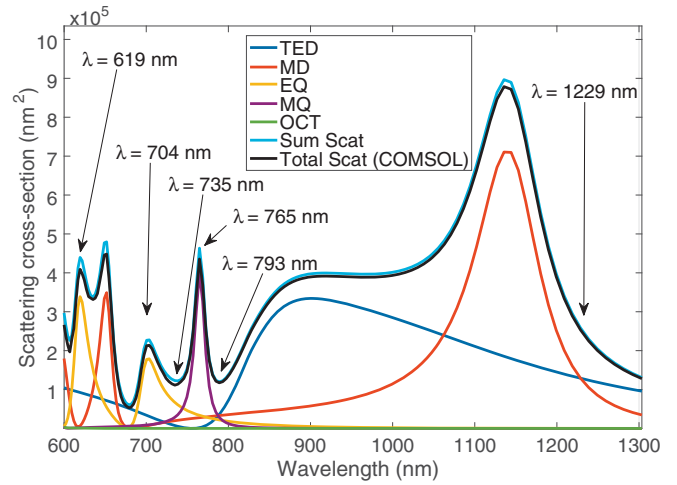


FIG. 2. Spectra of the scattering cross section and corresponding multipoles' contributions calculated for a silicon nanocube with height of $H = 250$ nm. “Sum Scat” is the sum of multipoles' contributions, Total Scat (COMSOL) is a scattering cross section obtained via direct numerical simulation; other abbreviations can be found in the text. The black arrows indicate the wavelengths, for which scattering patterns are presented in Fig. 3.

wave. Geometrical difference between the radiation patterns in Figs. 3(a)–3(c) is explained by the nonresonant contributions of other multipoles to the scattering process. For example, the difference between the radiation patterns is shown in Figs. 3(a) and 3(b), where the basic contribution is provided by the EQ scattering with contributions of ED, MD, and MQ moments. Note that these contributions are changed with changing of spectral points (see Fig. 2). Thus interference between the fields generated by the resonant and nonresonant multipolar moments can significantly affect the scattering directions. If the scattering cross section includes almost equal contributions of several multipole moments, as we show for wavelengths $\lambda = 735$ nm and $\lambda = 793$ nm in Fig. 2, then radiation patterns can have different shapes determined by the number and types of the multipoles. In the case of cubic silicon particles, it is possible to achieve a side-scattering effect, when the forward and backward scatterings are suppressed and the scattered waves basically propagate perpendicular to \mathbf{k} of the incident wave [Figs. 3(d) and 3(e)]. We found that for $\lambda = 735$ nm the cubic nanoparticle predominantly scatters light along the direction (E) corresponding to the incident wave polarization [Fig. 3(d)], whereas for $\lambda = 793$ nm [Fig. 3(e)] there is symmetric side scattering. Such effects are realized due to the interference between the waves radiated by the dipole and quadrupole multipole moments. Thus, if the contribution from dipoles and quadrupoles of both electric and magnetic types in the scattering cross section are identical as for $\lambda = 793$ nm in Fig. 2, then the isotropic side scattered pattern can be realized [Fig. 3(e)]. When only TED and MD moments provide the main and equal contributions in the scattering the Kerker or anti-Kerker effects can be realized depending on the TED and MD phases [19]. For example, for the considered cubic nanoparticles there is a strong suppression of the backward scattering (the Kerker effect) at $\lambda = 1229$ nm [see Figs. 2 and 3(f)].

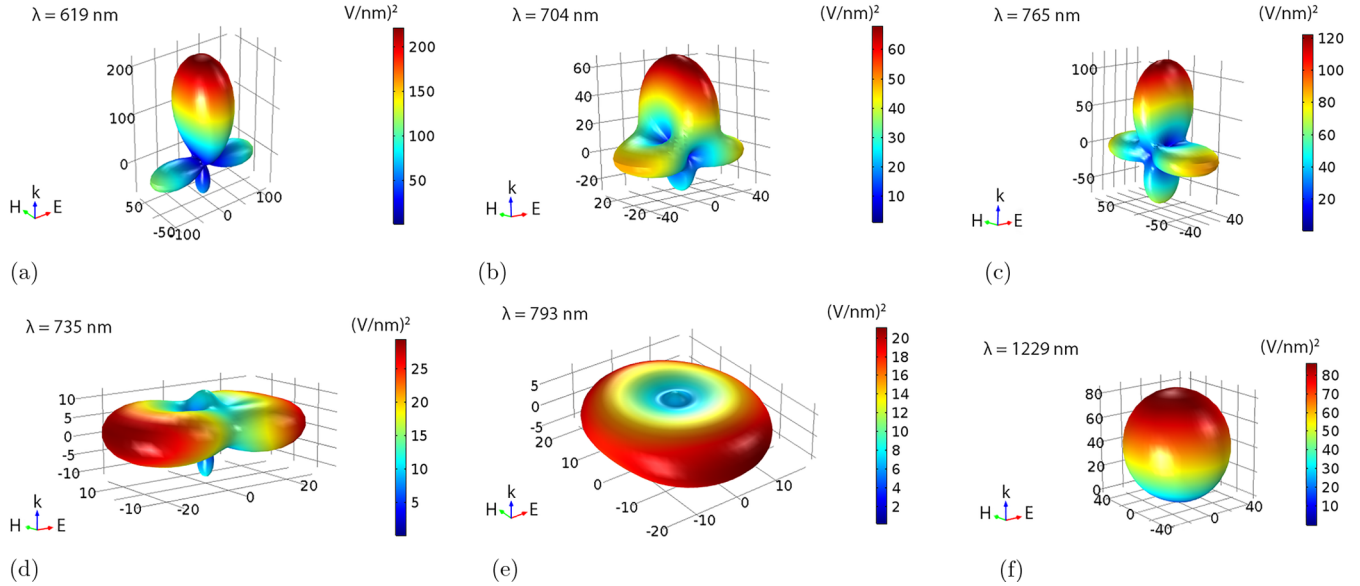


FIG. 3. Radiation patterns of the cubic nanoparticle with edge $H = 250$ nm calculated at the wavelengths indicated by the black arrows in Fig. 1. (a) $\lambda = 619$ nm, (b) $\lambda = 704$ nm, (c) $\lambda = 765$ nm, (d) $\lambda = 735$ nm, (e) $\lambda = 793$ nm, and (f) $\lambda = 1229$ nm. The incident linearly polarized plane wave.

Now let us consider the evolution of the multipole contributions to the light scattering cross sections for silicon parallelepipeds with base edge of $D = 250$ nm and varying heights H . We note that there is an ordinary behavior for the first (from the long-wavelengths side) TED and MD resonances: both resonances are redshifted with increasing the parallelepiped height H for the given incidence direction. It has been demonstrated in details in [22]. The evolution of the other dipole and quadrupole resonances with increasing H are demonstrated in Fig. 4. As the particle's height increases at the particular wavelength, the electromagnetic field distribution inside the particles becomes more inhomogeneous resulting in the excitation of higher order multipoles. Multipole resonances in Fig. 4 exhibit the redshift as H increases. Especially, this is concerned with the EQ and MD contributions. Since the shift values for EQ and MD resonances are different it is possible to get some spectral overlapping of these resonances when $H/D > 1$ [Fig. 4(c)]. Another evolution scenario is realized for the TED and MQ resonances in the considered spectral range. There is almost total overlapping of these resonances for the nanoparticles with $H/D < 1$ [$\lambda = 700$ nm in Fig. 4(a) and $\lambda = 735$ nm in Fig. 4(b)]. This overlapping provides the side scattering suppression as it is demonstrated by the insets in Figs. 4(a) and 4(b). However, the TED contribution into this TED-MQ resonance is decreased with increasing the H and totally disappears in the case of the nanocube ($\lambda = 770$ nm in Fig. 2). Moreover, in the case of $H/D > 1$ the MQ resonance is also significantly attenuated and its contribution to the scattering cross section becomes comparable with other multipoles that results in strong isotropic side scattering [the inset in Fig. 4(c)]. Note that the electric octupole contribution is negligibly small in all considered spectral range. Thus tuning the particle aspect ratio could allow one to get a transformation from the forward-backward scattering to the isotropic side scattering (insets in Fig. 4).

B. Pyramidal nanoparticles

In this section we consider pyramidal nanoparticles. Figure 5 presents the scattering cross-section spectra and corresponding multipole decompositions calculated for silicon nanopyramid (height of $H = 250$ nm and base edge of $D = 250$ nm) and different irradiation conditions. In contrast to the cubic nanoparticle, there is strong overlapping of MQ and TED resonances for both irradiation conditions ($\lambda = 568$ nm in Fig. 5). Similar to the case of the parallelepiped nanoparticles, when $H/D < 1$, the simultaneous resonant excitation of the MQ and TED moments provides strong suppression of the side scattering that is demonstrated in Fig. 6(b). However, predominant side scattering along the incident magnetic field polarization is realized for the $\lambda = 545$ and $\lambda = 622$ nm in Fig. 5(a) and, respectively, demonstrated in Figs. 6(a) and 6(c). Such complicated effects are realized due to the equal contributions of the dipole and quadrupole moments in the scattering. The Kerker effect is realized for $\lambda = 795$ nm [Figs. 5(a) and 6(d)] when the TED and MD contributions in the scattering cross section coincide (Fig. 5). The difference of the multipole decompositions for the different irradiation direction presented in Figs. 5(a) and 5(b) will be discussed in the final subsection of the article.

Spectral evolution of the multipole contributions to the light scattering cross sections for the silicon nanopyramids with varying height H is shown in Fig. 7. One can see that the resonant contributions of TED, MD, EQ, and MQ moments shift to the long-wavelengths side as values increase. Moreover, new resonant contributions can appear in the considered spectral range. In Fig. 7(b) one can note a feature concerning the TED contribution to the scattering. The first TED resonances (from the long wavelength side) have the small dips, located at the wavelengths of the first MD resonances in Fig. 7(a). Our multipole analysis shows that this feature can be attributed to the resonant excitation of the electric toroidal dipole (TD)

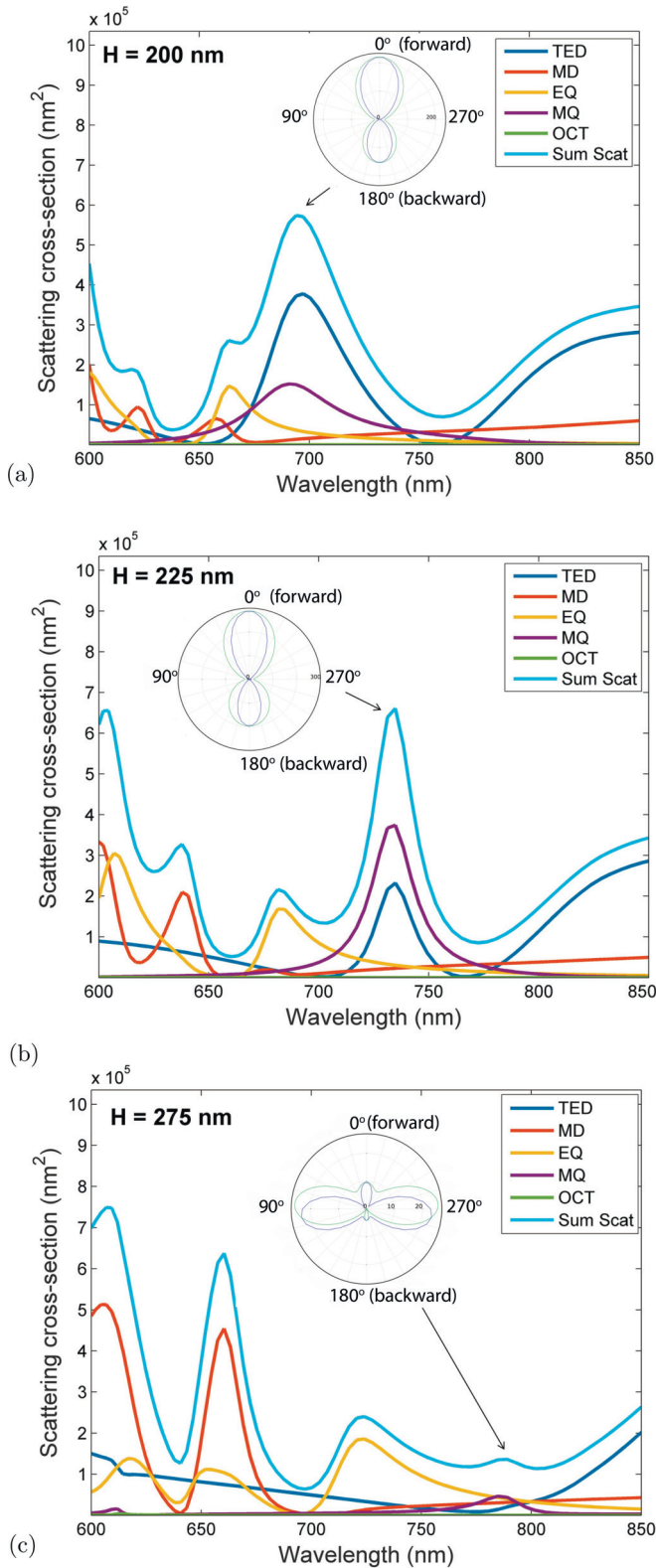


FIG. 4. Spectra of the scattering cross sections and corresponding multipole decompositions calculated for silicon nanoparallelepipeds with the base edge equal to 250 nm and the height $H =$ (a) 200 nm, (b) 225 nm, (c) 275 nm. The scattering cross section for the corresponding cubic nanoparticle is presented in Fig. 2. The insets are 2D presentations of corresponding scattering patterns: the green (blue) contour corresponds to the plane of the incident electric (magnetic) field polarization.

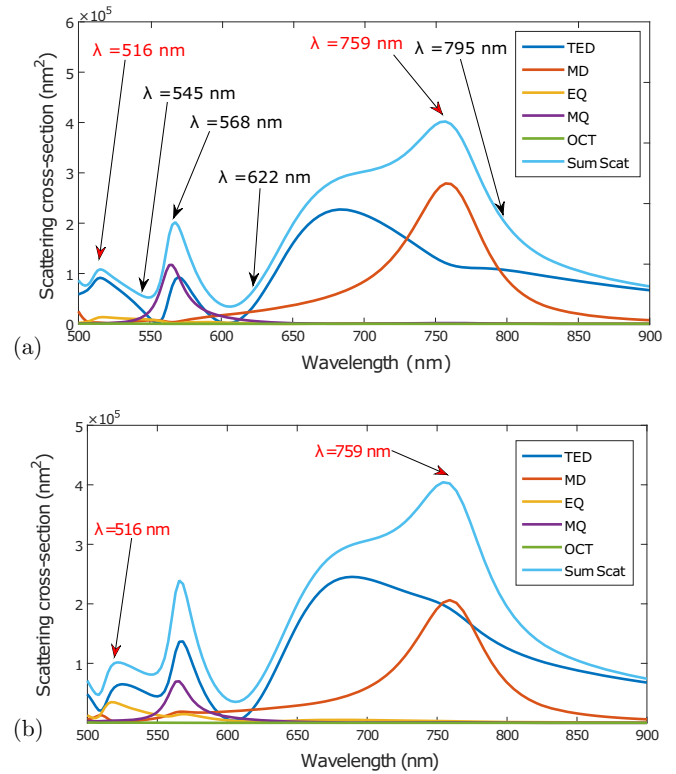


FIG. 5. Spectra of the scattering cross sections and corresponding multipoles calculated for the silicon nanopyramid (height of $H = 250$ nm; base edge of $D = 250$ nm). (a) The pyramid is illuminated by light plane waves from the pyramid base edge side. (b) It is illuminated from the pyramid top. The black arrows in (a) correspond to the spectrum points for which the scattering patterns are presented in Fig. 6. The red arrows correspond to the spectrum points for which the 2D scattering patterns are presented in Fig. 10.

moment at the same spectral point. Thus the dip of the first TED resonance in Fig. 7 ($\lambda = 720$ nm) is the result of the destructive interference between ED and TD contributions in

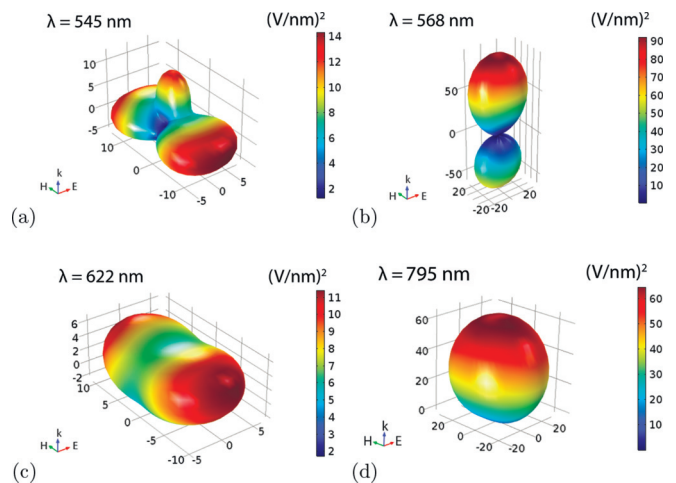


FIG. 6. Radiation patterns of the silicon pyramidal particle with height $H = 250$ nm and base edge $D = 250$ nm. (a) $\lambda = 545$ nm. (b) $\lambda = 568$ nm. (c) $\lambda = 622$ nm. (d) $\lambda = 795$ nm.

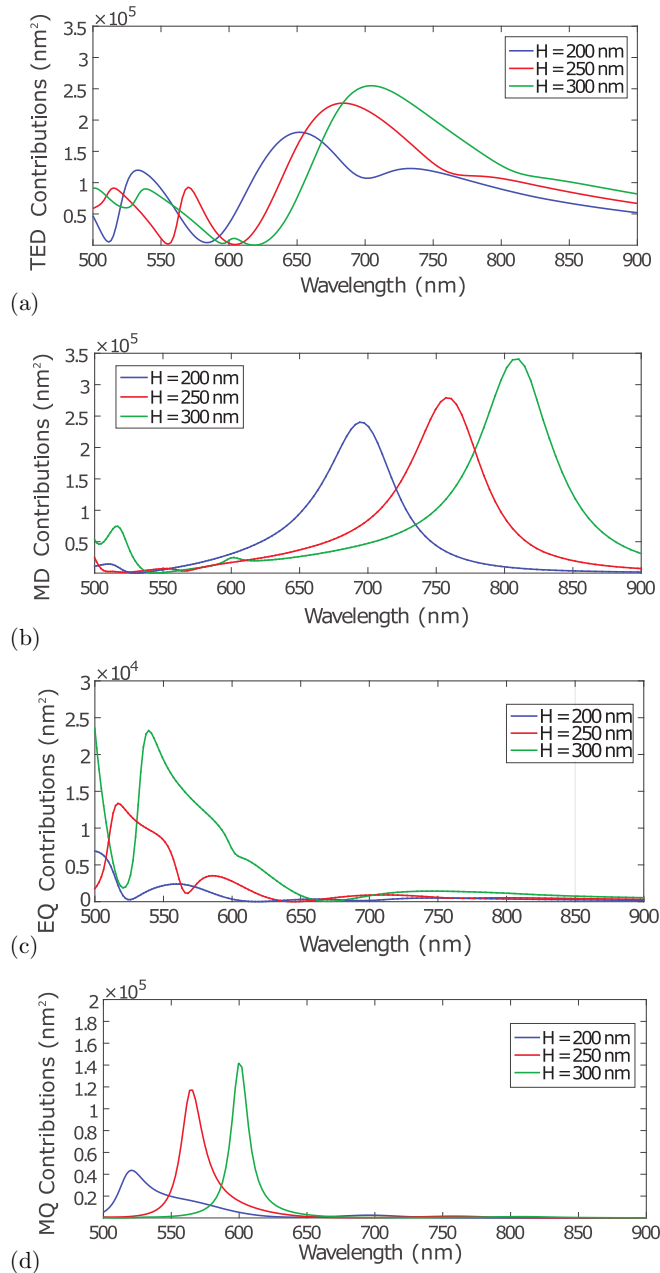


FIG. 7. Contributions of multipole moments to the scattering cross section spectra calculated for the silicon nanopillars (the base edge of $D = 250$ nm and height of H) irradiated from the bottom side. (a) TED contributions. (b) MD contributions (c) EQ contributions. (d) MQ contributions.

the TED moment [Eq. (11)] and therefore in the scattering [Eq. (10)].

C. Conical nanoparticles

Scattering cross section and corresponding multipole moments for a silicon nanocone presented in Fig. 8 is very similar to the scattering cross section for the nanopillar shown in Fig. 5(a). This similarity is explained by similar symmetrical properties of the particles and the fact that electromagnetic fields are basically concentrated in the particle volume. In the

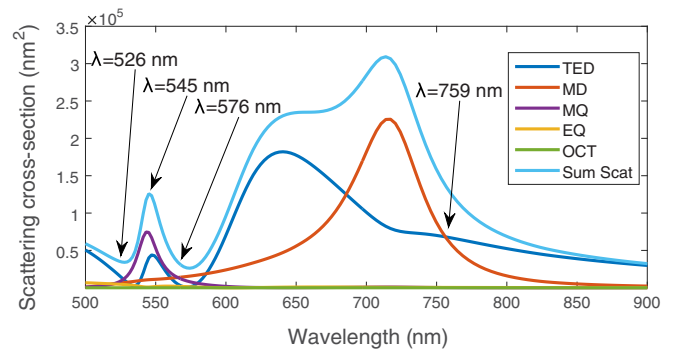


FIG. 8. Spectra of the scattering cross section and corresponding multipoles were calculated for the silicon nanocone (height of $H = 250$ nm; base diameter of $D = 250$ nm). The nanocone is illuminated by the light plane waves from the cone base side. Black arrows correspond to the spectrum points for which the scattering patterns are presented in Fig. 9.

case of the nanocone we also do not observe any realization of the single MQ resonance which takes place for the cubic nanoparticle (Fig. 2). Here the MQ resonance is combined with the TED resonance ($\lambda = 545$ nm in Fig. 8) providing almost total suppression of the side scattering, as it is shown in Fig. 9(b). Figures 9(a) and 9(c) demonstrate realization of the predominant side scattering at $\lambda = 526$ nm and $\lambda = 576$ nm. In these cases the dipole and quadrupole contributions are almost equal to each other. Depending on the field phases, they generate the side scattering which can be realized along mutually perpendicular directions. The Kerker effect presented in Fig. 9(d) is realized at $\lambda = 759$ nm (Fig. 8).

The spectral evolution of the multipole contributions to the light scattering cross sections for the conical nanoparticles as a function of their height is qualitatively similar to the considered pyramidal nanoparticles in Fig. 7.

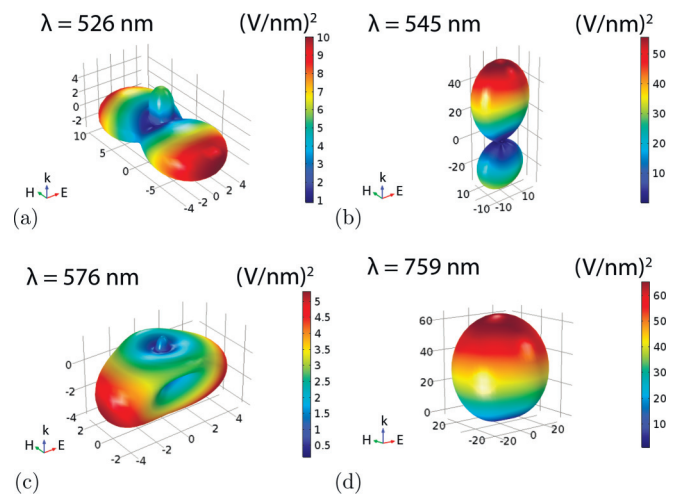


FIG. 9. Radiation patterns of the silicon conical particle with height $H = 250$ nm and diameter $D = 250$ nm. (a) $\lambda = 526$ nm. (b) $\lambda = 545$ nm. (c) $\lambda = 576$ nm. (d) $\lambda = 759$ nm.

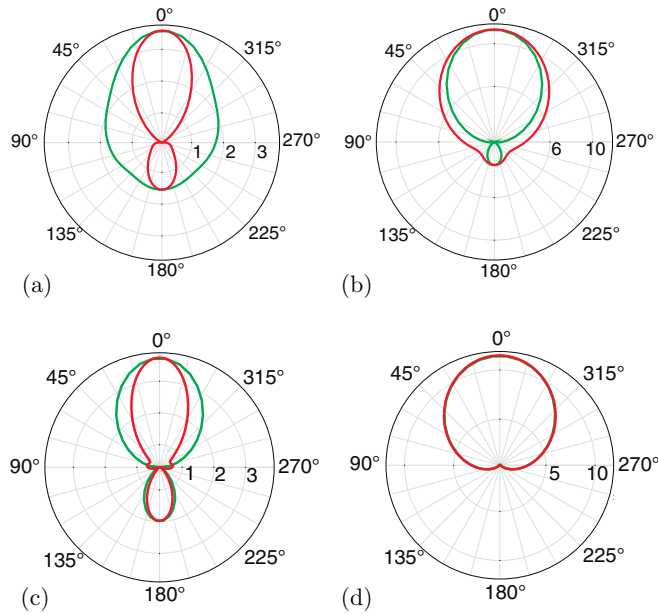


FIG. 10. 2D scattering patterns for the two different directions of the incident light for the silicon nanopyramid (height of $H = 250$ nm and base edge of $D = 250$ nm). (a) The incidence from the pyramid base, $\lambda = 516$ nm. (b) The incidence from the pyramid base, $\lambda = 759$ nm. (c) The incidence from the pyramid top, $\lambda = 516$ nm. (d) The incidence from the pyramid top, $\lambda = 759$ nm. Red (green) contour corresponds to the plane of the incident electric (magnetic) field polarization.

D. Influence of the light incidence direction

In the last subsection we consider the influence of the light incidence direction on the scattering by the pyramidal/conical nanoparticles with height of $H = 250$ nm and base edge/diameter of $D = 250$ nm. The multipole decomposition spectra of the scattering cross sections for the bottom side illumination and the top (reversed) side illumination of silicon nanopyramid have been shown in Fig. 5. One can see that despite the fact that the total scattering cross section does not change crucially, multipoles spectra are quite different. For the reversed illuminating [Fig. 5(b)] the electric type multipoles (TED and EQ) provide larger contributions to the scattering cross section, whereas the contributions of the magnetic type multipoles (MD and MQ) are attenuated. Note that this asymmetry is not the result of variation of coordinates of the point multipoles are attributed to. The multipoles are considered to be located at the scatterer center of mass in both illumination conditions. The influence of the light incidence direction is demonstrated in Fig. 10, where light scattering directivity (the scattering patterns) is shown for the two illumination directions and for the fixed light wavelengths. These wavelengths are marked in Fig. 5 with the red arrows.

One can see that the scattering pattern in Fig. 10(a) is basically determined by the TED scattering, whereas for the other incidence direction [from the pyramid top side and for the same wavelength, Fig. 10(c)] the scattering pattern is a combination of TED and EQ scattering. In the latter case the side scattering is suppressed due to the destructive interference between the fields generated by the TED and EQ. In Figs. 10(b)

and 10(d) one can see the result of the interference between the TED and MD scattered fields. In contrast to the case of the from-base incidence [Fig. 10(b)] in the case of the top incidence, the strong Kerker effect is realized around the wavelength of $\lambda = 759$ nm. Note that for the cone particles one can observe similar asymmetric behavior depending on the illumination conditions.

Importantly, this asymmetry effect can be used for different applications where the scatterer triggered properties controlled by the external illumination are needed, for example, functional bilateral nanoantennas, emitting light diodes, antireflective structures, and surface enhanced phenomena.

IV. CONCLUSION

In conclusion, using the multipole decomposition approach, the multipoles up to the third order that were excited by light in parallelepipedal, pyramidal, and conical silicon nanoparticles were investigated. It has been demonstrated that peculiar scattering patterns with certain predominant scattering directions can be obtained by tuning the spectral overlap of several multipoles. In particular, using cubic particles it is possible to get a strong isotropic side scattering with simultaneous suppression of the forward and backward scattering. In the case of the pyramidal and conical nanoparticles the total suppression of the side scattering can be realized due to the equal contributions of the total electric dipole and magnetic quadrupole moments in the scattered fields. It has been shown that the effect of the asymmetrical multipole response in conical and pyramidal particles depends on the illumination direction. Our investigation provides important information about the roles of the high order multipoles in the light scattering by nonspherical nanoparticles. The changing of the wave vector and the polarization from the chosen direction will affect the scattering properties of considered particles; this is the topic of our future work as well as periodic structures research. For instance, since the optical properties of the metamaterials are determined by the properties of their building blocks which are single resonators, we expect that the reciprocity feature will preserve in periodic arrays based on pyramidal or conical nanoparticles. The results obtained can be used for the development of the nanoantennas in the visible and near-infrared spectral ranges, creating metasurfaces and metamaterials, providing flexible control over light behavior, and for invention and realization of different coatings for optics and photovoltaics.

ACKNOWLEDGMENTS

This work has been supported by the Russian Fund for Basic Research within Projects No. 16-52-00112. The calculations of multipole moments have been supported by the Russian Science Foundation Grant No. 16-12-10287. Support has been provided by the Government of the Russian Federation (Grant No. 074-U01) and Deutsche Forschungsgemeinschaft (DFG) within the Project EV No. 220/2-1. A.S. acknowledges the support of the President of Russian Federation in the frame of Scholarship No. SP-4248.2016.1 and the support of Ministry of Education and Science of the Russian Federation (GOSZADANIE Grant No. 3.4982.2017/6.7). K.B. was

partially supported by FASIE. The research described was partially supported by the startup grant of A.K. at Ben-Gurion

University of the Negev and was performed as part of a joint Ph.D. program between the BGU and ITMO.

-
- [1] A. B. Evlyukhin, C. Reinhardt, A. Seidel, B. S. Lukyanchuk, and B. N. Chichkov, *Phys. Rev. B* **82**, 045404 (2010).
- [2] A. I. Kuznetsov, A. E. Miroshnichenko, Y. H. Fu, J. Zhang, and B. Luk'Yanchuk, *Sci. Rep.* **2**, 492 (2012).
- [3] A. B. Evlyukhin, S. M. Novikov, U. Zywiets, R. L. Eriksen, C. Reinhardt, S. I. Bozhevolnyi, and B. N. Chichkov, *Nano Lett.* **12**, 3749 (2012).
- [4] A. I. Kuznetsov, A. E. Miroshnichenko, M. L. Brongersma, Y. S. Kivshar, and B. Lukyanchuk, *Science* **354**, aag2472 (2016).
- [5] S. Jahani and Z. Jacob, *Nat. Nanotechnol.* **11**, 23 (2016).
- [6] A. A. Basharin, V. Chuguevsky, N. Volsky, M. Kafesaki, and E. N. Economou, *Phys. Rev. B* **95**, 035104 (2017).
- [7] A. A. Basharin, M. Kafesaki, E. N. Economou, C. M. Soukoulis, V. A. Fedotov, V. Savinov, and N. I. Zheludev, *Phys. Rev. X* **5**, 011036 (2015).
- [8] A. B. Evlyukhin, C. Reinhardt, and B. N. Chichkov, *Phys. Rev. B* **84**, 235429 (2011).
- [9] M. I. Stockman, *Opt. Express* **19**, 22029 (2011).
- [10] A. Karabchevsky, A. Mosayyebi, and A. V. Kavokin, *Light: Sci. Appl.* **5**, e16164 (2016).
- [11] A. E. Krasnok, A. E. Miroshnichenko, P. A. Belov, and Y. S. Kivshar, *Opt. Express* **20**, 20599 (2012).
- [12] D. Markovich, K. Baryshnikova, A. Shalin, A. Samusev, A. Krasnok, P. Belov, and P. Ginzburg, *Sci. Rep.* **6**, 22546 (2016).
- [13] V. Kozlov, D. Filonov, A. S. Shalin, B. Z. Steinberg, and P. Ginzburg, *Appl. Phys. Lett.* **109**, 203503 (2016).
- [14] K. V. Baryshnikova, A. Novitsky, A. B. Evlyukhin, and A. S. Shalin, *J. Opt. Soc. Am. B* **34**, D36 (2017).
- [15] A. Katiyi and A. Karabchevsky, *J. Lightw. Technol.* **35**, 2902 (2017).
- [16] N. Bontempi, K. E. Chong, H. W. Orton, I. Staude, D.-Y. Choi, I. Alessandri, Y. S. Kivshar, and D. N. Neshev, *Nanoscale* **9**, 4972 (2017).
- [17] P. Spinelli, M. Verschuuren, and A. Polman, *Nat. Commun.* **3**, 692 (2012).
- [18] M. Decker, I. Staude, M. Falkner, J. Dominguez, D. N. Neshev, I. Brener, T. Pertsch, and Y. S. Kivshar, *Adv. Opt. Mater.* **3**, 813 (2015).
- [19] M. Kerker, D.-S. Wang, and C. Giles, *JOSA* **73**, 765 (1983).
- [20] I. Staude, A. E. Miroshnichenko, M. Decker, N. T. Fofang, S. Liu, E. Gonzales, J. Dominguez, T. S. Luk, D. N. Neshev, I. Brener *et al.*, *ACS Nano* **7**, 7824 (2013).
- [21] I. Staude and J. Schilling, *Nat. Photon.* **11**, 274 (2017).
- [22] P. D. Terekhov, K. V. Baryshnikova, A. S. Shalin, A. Karabchevsky, and A. B. Evlyukhin, *Opt. Lett.* **42**, 835 (2017).
- [23] T. Das, P. P. Iyer, R. A. DeCrescent, and J. A. Schuller, *Phys. Rev. B* **92**, 241110 (2015).
- [24] E. D. Palik, *Handbook of Optical Constants of Solids* (Academic Press, New York, 1998), Vol. 3.
- [25] D. Sikdar, W. Cheng, and M. Premaratne, *J. Appl. Phys.* **117**, 083101 (2015).
- [26] A. B. Evlyukhin, T. Fischer, C. Reinhardt, and B. N. Chichkov, *Phys. Rev. B* **94**, 205434 (2016).
- [27] R. E. Raab and O. L. De Lange, *Multipole Theory in Electromagnetism: Classical, Quantum, and Symmetry Aspects, with Applications* (Oxford University Press on Demand, Oxford, 2005), Vol. 128.
- [28] A. E. Miroshnichenko, A. B. Evlyukhin, Y. F. Yu, R. M. Bakker, A. Chipouline, A. I. Kuznetsov, B. Lukyanchuk, B. N. Chichkov, and Y. S. Kivshar, *Nat. Commun.* **6**, 8069 (2015).
- [29] N. A. Nemkov, I. V. Stenishchev, and A. A. Basharin, *Sci. Rep.* **7**, 1064 (2017).
- [30] M. V. Cojocari, K. I. Schegoleva, and A. A. Basharin, *Opt. Lett.* **42**, 1700 (2017).
- [31] C. F. Bohren and D. R. Huffman, *Absorption and Scattering of Light by Small Particles* (John Wiley & Sons, New York, 2008).
- [32] E. E. Radescu and G. Vaman, *Phys. Rev. E* **65**, 046609 (2002).
- [33] L. D. Landau and E. M. Lifshitz, *The Classical Theory of Fields* (Pergamon Press, New York, 1971).
- [34] M. Y. Ali, W. Hung, and F. Yongqi, *Int. J. Prec. Eng. Manufact.* **11**, 157 (2010).
- [35] M. I. Tribelsky, J.-M. Geffrin, A. Litman, C. Eyraud, and F. Moreno, *Sci. Rep.* **5**, 12288 (2015).